PERGAMON

Deep-Sea Research II 45 (1998) 2637–2664

DEEP-SEA RESEARCH
PART II

Chemical variations of hydrothermal particles in the 1996 Gorda Ridge Event and chronic plumes[1]

R.A. Feely*, E.T. Baker, G.T. Lebon, J.F. Gendron, G.J. Massoth, C.W. Mordy

Pacific Marine Environmental Laboratory, National Oceanic and Atmospheric Administration, 7600 Sand Point Way N.E., Seattle, WA 98115-0070, USA

Received 20 May 1997; accepted 13 April 1998

Abstract

In response to the 1996 magmatic intrusion on the Gorda Ridge near 42.68°N, 126.78°W in late February, we conducted three cruises to the region in March, April, and June. On all three cruises particulate samples were collected, along with CTD/nephelometer data and total dissolved Fe and Mn samples. During each cruise, we collected samples from large oblate spheroid-shaped event plumes. These event plumes had long axis diameters of about 10–15 km and ranged in depth from about 1800 to 2700 m. A strong linear correlation between nephelometer voltage and particulate Fe allowed us to estimate the total amount of particulate Fe in the event plumes at approximately 20×10^6 moles of Fe, or $\sim 28\%$ of the Fe in the 1986 megaplume on the Cleft Segment of the Juan de Fuca Ridge. We observed significant decreases in particulate Cu and Zn concentrations ($> 100\%$ decrease in Cu/Fe and Zn/Fe ratios) between the Gorda Ridge event plumes. These results suggest that each of the two event plumes originated from a chemically distinct source fluid. Fe ferrihydrite particles maintained a constant ratio of coprecipitated oxyanion species in the two event plumes. Based upon the chemical inventories for particulate Fe, P, and V, we suggest that event plumes might play a small role in the geochemical budgets for these elements.

1. Introduction

On 28 February 1996, intense seismicity was detected in the northeast Pacific Ocean using the T-phase Monitoring System developed by NOAA/PMEL to access

* Corresponding author. Tel.: 00 1 206 526 6214; fax: 00 1 206 526 6744; e-mail: feely@pmel.noaa.gov.

[1] Contribution numbers 1857 from the Pacific Marine Environmental Laboratory of NOAA and 469 from the University of Washington Joint Institute for the Study of the Atmosphere and Oceans.

0967-0645/99/$ – see front matter
PII: S0967-0645(98)00087-3

the U.S. Navy's SOund SUrveillance System (SOSUS) in the northeast Pacific (Fox and Dziak, 1998). The event was located on the northernmost segment of the Gorda Ridge near 42.68°N, 126.78°W. The intense seismic activity lasted for about 3 weeks, ending on 20 March 1996. Camera work and SeaBeam studies indicated that the seismic activity was caused by seafloor eruptions of lava which added 0.02 km^3 of fresh material at the sea floor (Chadwick et al., 1998). A smaller SeaBeam anomaly centered at 42.61°N, 126.82°W was just north of an axial seamount. A burst of T-phase seismicity from 10 to 20 March was roughly coincident with the smaller anomaly. The Gorda Ridge eruption had many of the same characteristics of the previously monitored eruption at Coaxial Segment of the Juan de Fuca Ridge (Baker et al., 1994; Massoth et al., 1995; Embley et al., 1994; Baker et al., 1998) and, therefore, it provided an excellent opportunity to study physical and chemical changes of hydrothermal particles that occur in event plumes during and after an eruption.

Hydrothermal circulation of seawater through the global ridge crest system is the principal agent for the transfer of heat and chemicals between the oceanic crust and the overlying waters. This hydrothermal circulation is most concentrated at the ridge axes, where episodic intrusions of mantle magma create new ocean crust. Discharging vent fluids with temperatures from a few degrees to over 400°C rise buoyantly for tens to hundreds of meters, eventually forming dilute, neutrally buoyant plumes that spread laterally by local currents. Within the plumes, metal-rich sulfide, sulfate, and oxide precipitates form (Haymon and Kastner, 1981; Mottl, 1983; Campbell and Gieskes, 1984; Leinen, 1985; Feely et al., 1987, 1990, 1991, 1992, 1994a, b, 1996; Trocine and Trefry, 1988; Trefry and Metz, 1989; Campbell, 1991; Metz and Trefry, 1993; Kadko et al., 1994). The balance between sulfide and oxide minerals in the plume depends on metal and H_2S concentrations in the vent fluids. When the H_2S content in the vent fluids is high relative to Fe and other metals, the sulfide mineral phases dominate the particle distribution in the buoyant plume. Precipitation of these phases occurs shortly after mixing with seawater before concentrations of reacting species drop below pertinent solubility products. In contrast, precipitation of hydrous iron and manganese oxides occurs for some time in the buoyant and neutrally buoyant hydrothermal plumes because their solubility products are much lower. Trace element concentrations in all of these precipitates can be altered over time by reactions such as scavenging and oxidative dissolution (Feely et al., 1987, 1990a, b, 1992; Dymond and Roth, 1988; Trocine and Trefry, 1988; Trefry and Metz, 1989; German et al., 1990, 1991a, b; Metz and Trefry, 1993). While the distribution and composition of hydrothermal precipitates have been studied in steady-state hydrothermal plumes, we have very little information about the evolution of hydrothermal particles following a seafloor eruption.

In response to the 1996 seafloor eruption on the Gorda Ridge in late February (Fox and Dziak, 1998), a group of scientists formed the Gorda Ridge Event Assessment Team (GREAT) and conducted three cruises (hereafter referred to as GR1, GR2, and GR3) to the region to study the physical, chemical, and biological characteristics of the hydrothermal plumes (*McArthur*, 7–15 March, *Wecoma*, 6–16 April, and *Discoverer*, 10–25 June). On all three cruises particulate samples were collected, along with CTD/nephelometer data and total dissolvable Fe and Mn samples. During each

cruise, we were able to sample one of two large oblate spheroid-shaped event plumes. These plumes had a diameter of about 10–15 km and extended from about 1800 to 2700 m in the water column (Baker, 1998). Our sampling procedure consisted of a series of tow-yos and vertical casts. The package included a Sea Bird 911plus CTD sensor and nephelometer to transmit continuous hydrographic and optical data; an in situ chemical sensor; and a rosette of 19-L PVC sampling bottles for collecting discrete samples of various dissolved and particulate hydrothermal species. We conducted continuous measurements of Mn and Fe via in-situ flow injection analysis on the first two cruises, and shipboard measurements of Mn and Fe, using discrete samples collected with the rosette bottles (Massoth et al., 1998). Samples were also collected for shore-based analysis of helium isotopes, trace metals, nutrients, and suspended particles. In this paper, we report the results of the suspended matter chemistry and morphology data from that survey.

2. Geographic setting

The Gorda Ridge is a northeast-southwest trending spreading center approximately 250 km off the coast of southern Oregon and northern California (Fig. 1). The northern segment extends 68 km southward from the Blanco Fracture Zone and is characterized by high valley walls (600–1400 m) and an intermediate spreading rate of approximately 5.5 cm yr^{-1} (Riddihough, 1980). Hydrothermal plumes have been observed extending from 2300 to 3000 m at the GR14 site (42.76°N, 126.73°W), the GR15 site (42.95°N, 126.55°W), and the Sea Cliff hydrothermal field (42.76°N, 126.71°W) (Baker et al., 1987; Rona et al., 1990). The axial valley contains significant amounts of terrigenous, biogenic, volcanic and hydrothermal sediments (Karlin and Lyle, 1986).

3. Sampling methods

Neutrally buoyant plume particles were sampled using 19-L PVC water sampling bottles. The bottles were equipped with two separate sampling stopcocks. The first stopcock was attached about one-third up the side of the bottle from the bottom and was used to sample for gases, biology, and other non-filtered samples. The second stopcock was attached at the very bottom of the bottle and was used to collect water for particulate and dissolved trace metal samples. This stopcock was set off to the side of the center of the bottle with the flow pattern inside the bottle machined to resuspend particles that might have settled to the bottom or adhered to the sides of the bottle. Sample bottles were coated with teflon and used silastic internally for closure. The bottles were fixed to a 24-position General Oceanics™ rosette sampling system.

The rosette was towed in a saw-toothed pattern (tow-yo) between approximately 1700 m and about 10 m above the bottom. Sample depths over and immediately adjacent to the ridge axis were chosen on the basis of real-time observations of hydrothermal temperature and nephelometer intensity. Off-axis sample depths were

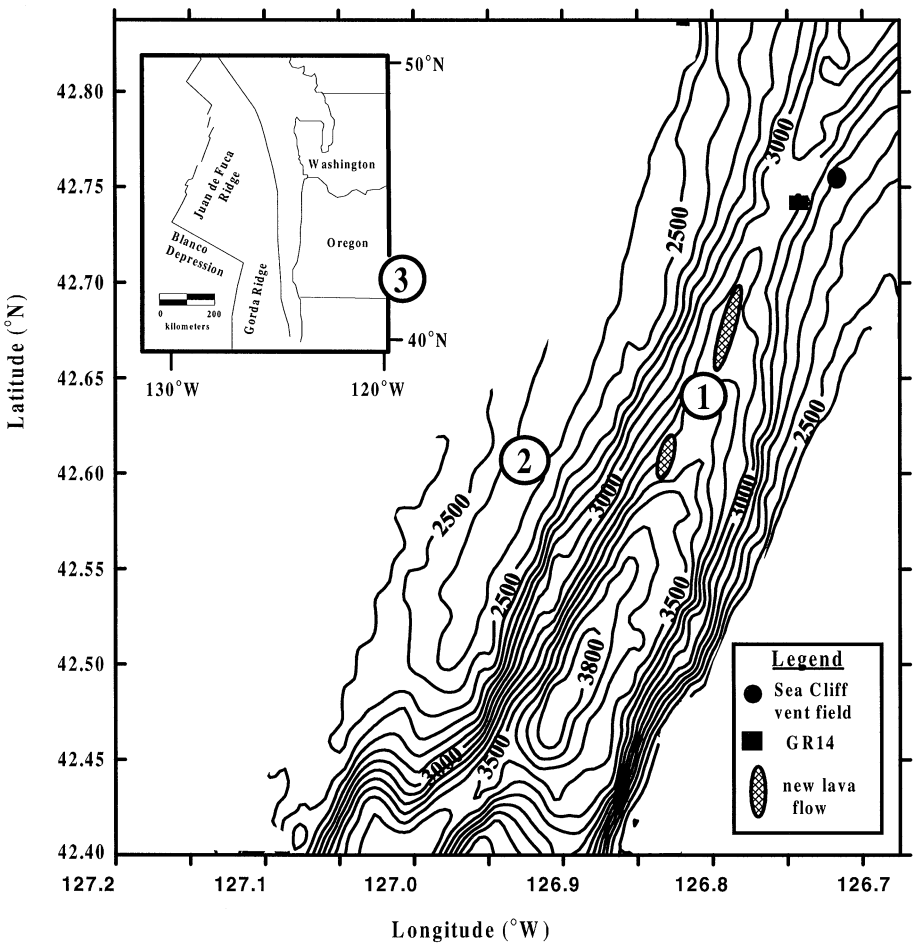

Fig. 1. Bathymetric map of the northern Gorda Ridge with the locations of the recent lava flows. The locations of the center of the event plumes for the GR1, GR2, and GR3 cruises are identified as 1, 2, and 3, respectively.

centered around the potential density interval that contained the ridge crest hydrothermal plumes.

Upon retrieval of the rosette system, gas and unfiltered samples were drawn from the middle stopcock. This was to ensure that large particles were not lost from the water samples (Gardner, 1977). After all the gas and nonfiltered samples were drawn, the remaining water was pressure filtered with filtered nitrogen (14 PSI). Samples were filtered onto preweighed, acid-cleaned Nuclepore™ filters (0.4 μm). The samples were rinsed in order to remove the sea salts in a laminar flow bench from 2 to 4 times with distilled-deionized (Milli-Q) water (18 K mho) that had been adjusted to pH 8 with

NH_4OH. Gentle vacuum was applied to remove the rinsings. They were then put into individual petri slides, dried in an evacuated desiccator over silica gel, and stored under vacuum until elemental analysis could be performed in the laboratory.

4. Analytical methods

4.1. Particle morphology

To determine phase chemistry and morphology of minerals on the particulate samples, an ISI DS130S Scanning Electron Microscope (SEM) equipped with a Kevex™ SuperQuantum Extra detector with an ultra thin window was used at 6–20 kV and from 300 to 65000X. Sections of the samples on Nuclepore™ filters were adhered to the tops of aluminum stubs with super glue. Samples were then sputter coated with a film of palladium for electrical conductivity. Qualitative analysis was performed on many samples using a Kevex Super Model 8000 microanalyzer, interfaced to the above mentioned SEM. Particle size analysis of individual particles and aggregates in the fields was determined using Kevex Features Analysis™ software (Feely et al., 1991a).

4.2. Elemental composition of the particles

Total elemental composition (Al, Si, P, S, K, Ca, Ti, Ba, V, Cr, Mn, Fe, Cu, Zn, and As) of the particulate matter was determined by X-ray primary- and secondary-emission spectrometry using a Kevex Model 8000–770 X-ray energy spectrometer with a rhodium X-ray source and using Mo, Se, and Co secondary targets. A non-destructive thin film technique (Baker and Piper, 1976; Holmes, 1981; Feely et al., 1991a) was used. Standards were prepared from suspensions of finely ground U.S. Geological Survey Rocks BHVO-1, GXR-1, GXR-2, GXR-4, and GXR-6, U.S.G.S. Marine Sediment MAG-1, National Bureau of Standards Rock and Sediment NBS-1633a and NBS-1645, National Research Council of Canada Sediment MESS-1, and Institute of Geophysical and Geochemical Exploration River Sediments GSD-1, GSD-5, GSD-6, and GSD-7, suspended on Nuclepore™ filters identical to those used for sample acquisition. The determination limits at normal loadings were less than 0.03 weight percent and 30 ppm for the major and trace elements, respectively (Feely et al., 1991a). The precision averaged 2% for the major elements except for sulfur, which averaged 11%, and 7% for the trace elements.

4.3. Dissolved phosphate

Dissolved reactive phosphate was determined from frozen samples at the Pacific Marine Environmental Laboratory using an Alpkem RFA3 Continuous Flow Analyzer. All samples were prefiltered through 0.4 μm acid-cleaned Nuclepore™ filters. The average precision of the analyses was 0.010 μmol/l, based upon multiple replicate analyses.

4.4. Factor analysis

Q-mode factor analysis is a statistical method of pattern recognition that is useful in extracting information from large data sets. It finds the principal factors, or "endmembers", that account for the variance in the data set. To determine the composition of the endmembers in a data set, the *Q*-mode factor analysis employs a vector rotation scheme to identify endmembers and the relative importance of each element to the endmembers. *Q*-mode factor analysis was used to distinguish hydrothermal from hydrogenous, biogenous, and diagenetic components of sediments east and west of the SEPR (Heath and Dymond, 1977; Leinen and Pisias, 1984). The program used to compute the primary factors in our data set was introduced by Klovan and Imbrie (1971) and modified for an oblique solution by Clarke (1978). The oblique solution is important because it ensures that the loadings for each sample can be interpreted as mixtures of endmember concentrations.

5. Results

5.1. Total suspended matter distributions

The distributions of nephelometer intensity and total suspended matter (TSM) concentrations over the study region indicate increases in suspended matter in the deep water from about 1800 to 3100 m, with event plumes as high as 1000 m above the seafloor (Baker, 1998). Hydrothermal plumes were readily identified by near-bottom increases in nephelometer intensity (in volts) produced by hydrothermally derived mineral precipitates. During the GR1 cruise (7–15 March; Fig. 2), TSM concentrations increased from background concentrations of about 10 μg/l at depths shallower than 1700 m to a maximum of 75 μg/l at about 2100 m from about 42.61°N to about 42.71°N along the west wall of the ridge axis immediately above the new lava flow at 42.68°N. Certainly the most interesting area surveyed was centered at about 42.63°N, where the event plume (EP96A) reached maximum thickness ($\sim$ 900 m). A second smaller steady-state "chronic" plume to the north at about 42.74°N was somewhat deeper and thinner with lower TSM concentrations (maximum TSM = 32 μg/l).

Observations during the GR2 cruise (6–16 April) found no evidence of an event plume at the EP96A site. The only evidence in the water column of the lava eruption at that site was a weak TSM plume within 250 m of the seafloor (Fig. 3a). About 6 km to the south, however, a distinct plume with TSM concentrations as high as 35 μg/l was found centered at a depth of about 2650 m (Fig. 3a and b). It is possible that this chronic plume was generated by a secondary release of hydrothermal emissions from the lava flow site at 42.68°N (Massoth et al., 1998). Directly above the western edge of this plume was another plume layer overlying the western axial wall (Fig. 3b). ^{3}He/heat ratios in this plume identify it as a part of an event plume (EP96B, Baker, 1998). Time constraints during the GR2 cruise prevented a complete mapping of this plume, but it was tagged with a RAFOS float (Lupton et al., 1998) and investigated more fully during GR3.

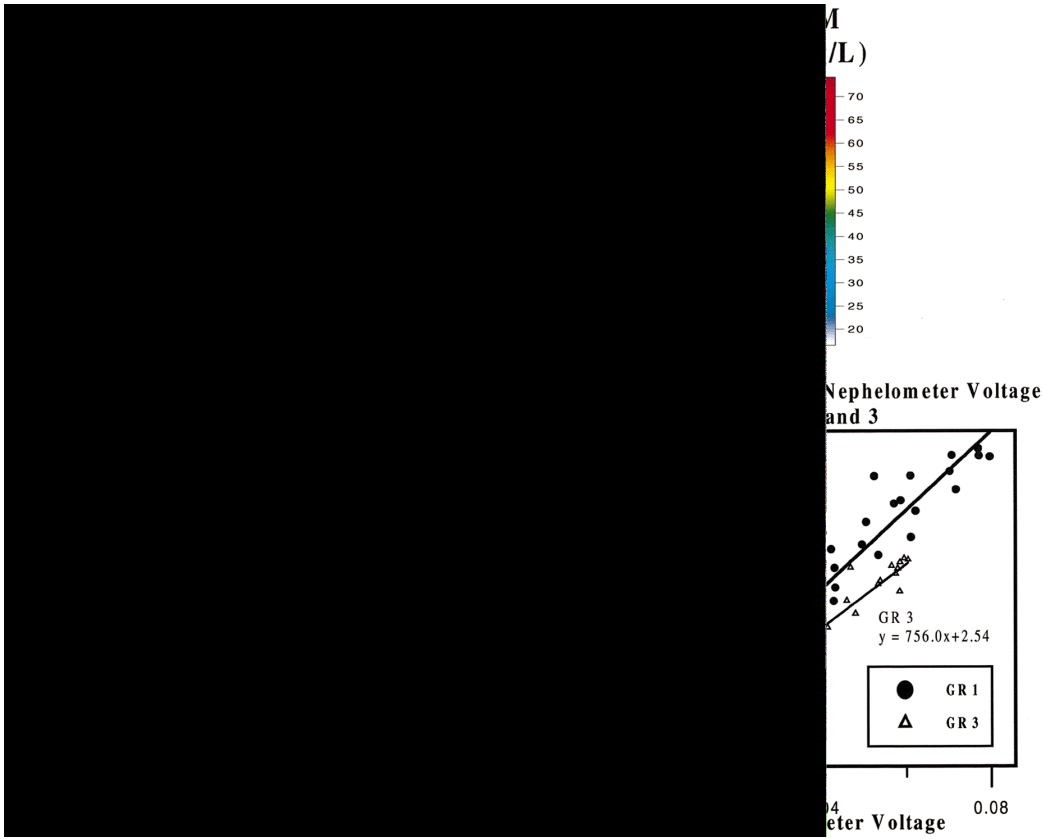

Fig. 2. (A) Distribution of total suspended matter (TSM) concentrations based over the study region from 1800 m to the seafloor for the GR1 cruise (*McArthur*, 7–15 March 1996). The large plume to the south is the event plume centered at about 2100 m and the smaller chronic plume at 2500 m to the north is a chronic plume of hydrothermal Mn particles and detrital mineral matter. (B) Cross-section of TSM across the ridge axis along 42.68°N. (C) Plot of total suspended matter (TSM) versus nephelometer intensity for the GR1 and GR3 cruises.

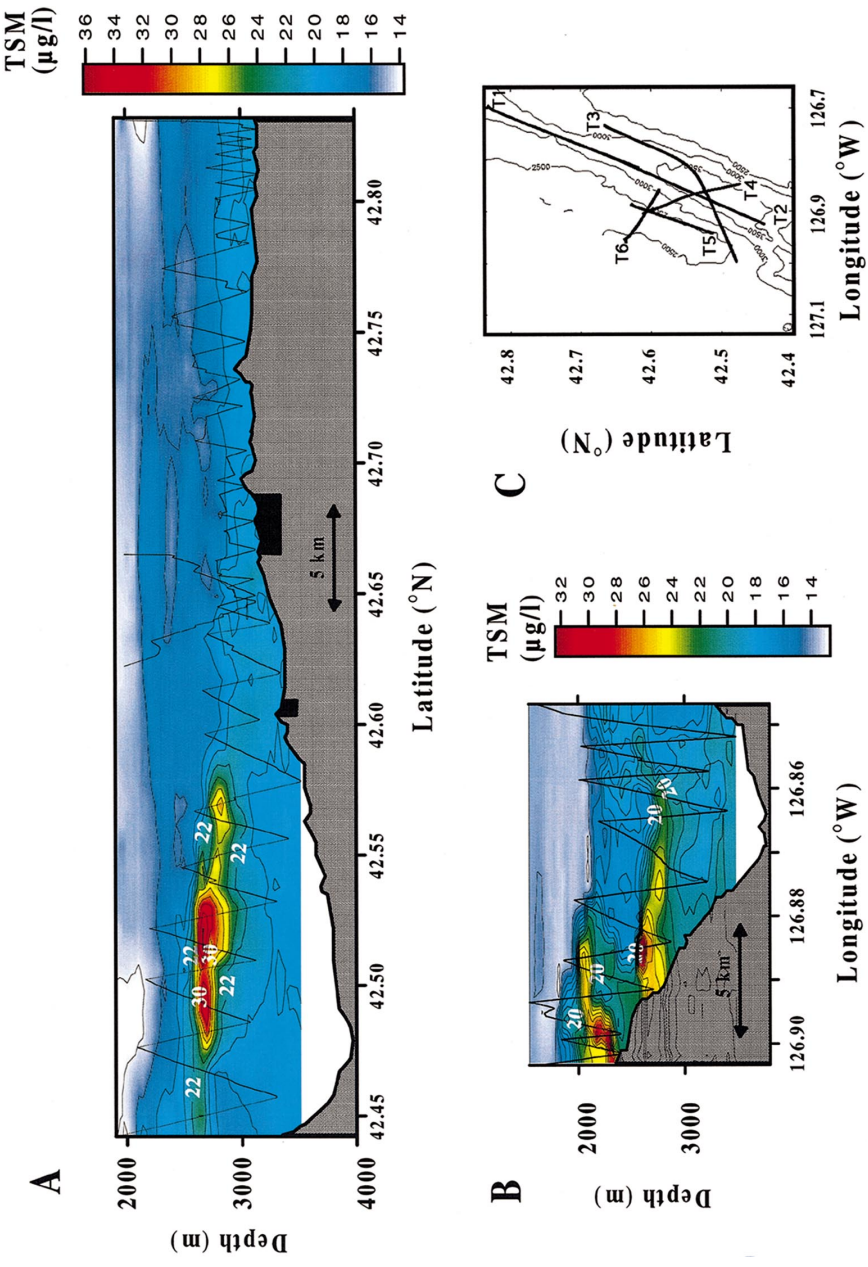

Fig. 3. Vertical sections of TSM along the primary axis (A) and cross axis (B) for the event and chronic plumes during the GR2 cruise (*Wecoma*, 6–16 April 1996). The cruise tracks are shown in (C). The primary axis tow in (A) are combined from T1 and T2, and the cross-axis tow in (B) is from T4.

Over the original lava flow at 42.68°N, TSM concentrations were only slightly elevated in the bottom 250 m of the water column, very similar to background concentrations to the north (Fig. 3a). Since the entire region has a persistent bottom nepheloid layer, due to local resuspension of bottom sediments due to local tidal currents, the enrichment of TSM over the original lava flow from residual venting at the lava flow site is somewhat masked by tidal mixing of the nepheloid layer in the region of the flow.

Observations during GR3 confirmed that EP96B, the shallow plume during GR2, was an event plume distinct from EP96A observed during GR1 (Baker, 1998). The center of EP96B was located beyond the west wall of the ridge axis, approximately 9 km WNW of the original location of EP96A (Fig. 4). Based on the tow-yo paths this was the most comprehensively sampled event plume of the three cruises. The shape of the plume is that of an elongated oblate spheroid with a long axis of approximately 15 km. TSM concentrations reached a maximum of 46 μg/l at approximately 2100 m centered at 42.69°N, 126.97°W. The plume thickness was approximately 700 m, from about 1800 to 2500 m. A plot of TSM versus nephelometer intensity for the GR1 and GR3 event plumes indicates two distinct data groupings which are significant at the 95% level (Fig. 2c). The enrichment of suspended matter concentrations within the event plume is primarily due to hydrothermal iron ferrihydrite particles. The offset between the GR1 and GR3 trends is probably the result of a change in background particle population between the spring GR1 cruise and the summer GR3 cruise (see below).

5.2. Particulate Al, Si, S, K, Ca, Ti, Mn, and Fe

Particulate Al, Si, P, S, K, Ca, Ti, Ba, V, Cr, Mn, Fe, Cu, Zn, and As (PAl, PSi, PP, PCa, PTi, PBa, PV, PCr, PMn, PFe, PCu, PZn, and PAs) concentration averages are given in Table 1. These elements are important constituents of hydrothermal phases, biogenic debris, and inorganic detrital material in the suspended matter. Al, K, and Ti are characteristic indicators of inorganic detrital phases, either resuspended mineral matter or basalt fragments from fresh lava with little contribution from hydrothermal precipitates. Si is a major constituent of diatom tests as well as of inorganic mineral matter and hydrothermal material, Ca is a major component of calcium carbonate tests, and Mn and Fe are major constituents of hydrothermally derived ferrihydrite particles (Campbell, 1991). The elemental ratios of these elements to each other help to determine the relative abundances of the different particle phases in the samples. For example, the GR1 chronic plume Fe/Al ratio in the particles is close to the value of the local sediments (Table 1), whereas EP96A has a strong enrichment of the particulate Fe/Al ratios (Fig. 5). This enrichment is characteristic of hydrothermally derived Fe ferrihydrite particles within the event plume. In contrast, the small chronic plume in Fig. 2a at GR1 V10 and GR1 V13 contains large amounts of resuspended detrital mineral particles consisting of aluminosilicate material (Table 1). As the GR1 event plume formed, the detrital components of the chronic plume and resuspended sediments were entrained into the event plume, causing an increase in the particulate Al, K, and Ti concentrations within the event plume. Based upon the Fe/Al ratios for the

sediments and event plume samples, we can estimate the mass of resuspended PFe in the GR1 event plume. By multiplying the mean PAl concentration of 63 nmol/l in the event plume by the Fe/Al ratio for the underlying sediments (~ 0.39; Karlin and Lyle, 1986), we estimate that the GR1 event plume contains an average of approximately 25 nmol/l of resuspended PFe. This amount of PFe is approximately 11% of the total mean PFe in the event plume. The remaining PFe consists of Fe ferrihydrite particles resulting from rapid oxidation of dissolved Fe in the event plume (Massoth et al., 1998).

Particulate Mn concentrations are low (< 2.0 nmol/l) in both event plumes. The concentration of PMn in the chronic plume and background nepheloid layer can be observed as an enrichment of the Mn/Al ratio versus depth in Fig. 5a. In this region, resuspension and horizontal advection of Mn-enriched bottom sediments caused these enrichments in the suspended matter of the chronic plumes. The Mn/Al and Fe/Al ratios within the chronic plume are similar to ratios observed in background suspended matter at GR1 V1 and GR1 V2 (Fig. 2), and also measured in background samples over the same region in 1985 (Fig. 5a and b). The low PMn concentrations within the GR1 event plume is indicative of a newly formed hydrothermal Fe ferrihydrite precipitate which has not yet been enriched with the more slowly precipitating hydrous manganese oxides (Cowen et al., 1990, 1991; Feely et al., 1992; Cowen et al., 1998). The higher Mn/Al ratios in the background and chronic plume particles is probably the result of increased bacterial activity at the seafloor from low-temperature hydrothermal activity (Cowen et al., 1990, 1991). This low-temperature vent-derived Mn would precipitate onto the resuspended sediment and/or sediments, thus enriching the PMn concentrations within the chronic plume particles.

The opposite trend in the Fe/Al ratio also indicates entrainment of resuspended sediments into a predominantly Fe-rich hydrothermally derived event plume. The Fe/Al ratio for EP96A ranges from 2 to 6. In nearly pure Fe-rich hydrothermally derived event plumes from the Juan de Fuca Ridge (EP86A and EP93A) the Fe/Al ratio ranges from 20 to 55 (R. Feely, unpublished data). Resuspension and entrainment of bottom sediments into the EP96A enriches the aluminosilicate fraction in the event plume and lowers the overall Fe/Al ratio. The enriched Al/Fe, K/Fe, and Ti/Fe ratios in EP96A samples relative to the CoAxial Segment event plume from the Juan de Fuca Ridge also demonstrates the impact of this entrainment process when a background nepheloid layer is present (Table 1). These ratios in the background and chronic plume samples are significantly higher than the event plume samples, signifying an entrainment of bottom sediments into the event plume. Clearly, the Gorda Ridge event plumes are contaminated with entrained chronic plume particles and resuspended sedimentary particles. The recent modeling work by Lavelle (1995) suggests that upward convective flow within the lower portions of an event plume will have sufficient vertical velocity to entrain particles from chronic plumes and resuspended sediments several hundreds of meters from the source.

Within the data sets from the three cruises there is a high degree of correlation between PFe and nephelometer intensity ($r^2 = 0.92$) (Fig. 6a), indicating that the plumes consist mainly of Fe-bearing phases including Fe ferrihydrite particles and resuspended sediments. Analytical scanning electron microscopy of filtered material

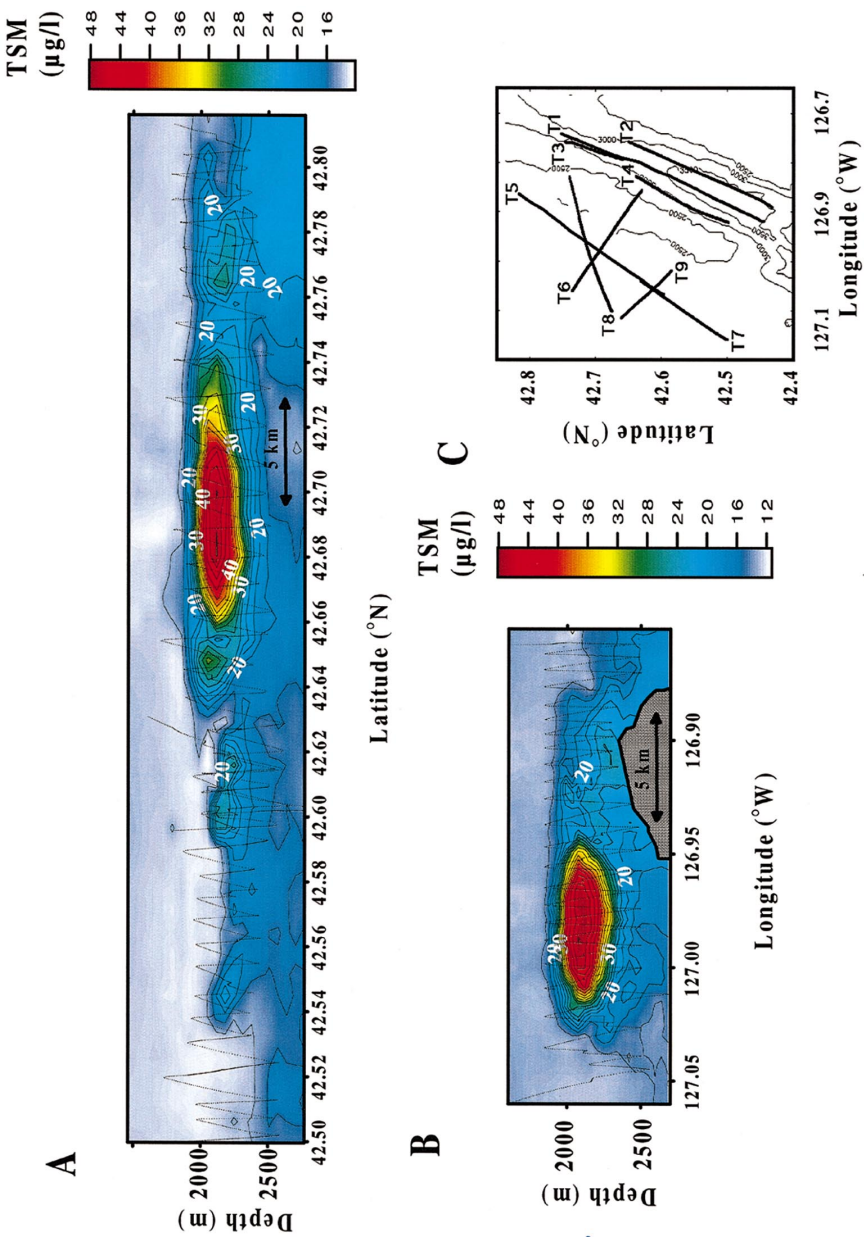

Fig. 4. Vertical sections of TSM along the primary axis (A) and cross axis (B) for the event and chronic plumes during the GR3 cruise (*Discoverer*, 10–25 June). The cruise tracks are shown in (C). The SW–NE tow in (A) are combined from T5 and T7, and the cross-axis tow in (B) is from T6.

Table 1
Mean concentrations and element/Fe ratios for particulate samples from the GR1, GR2, and GR3 cruises. Uncertainities are calculated at the ± 1 standard deviation level

Species	GR1 Background Samples mean concentration ($n = 8$)	GR1 Event Plume EP96A mean concentration ($n = 19$)	GR1 Chromic Plume mean concentration ($n = 5$)	GR2 Event Plume EP96B mean concentration ($n = 9$)	GR3 Background Samples concentration ($n = 2$)	GR3 Event Plume EP96B mean concentration ($n = 39$)	CoAxial Segment, JdFR Event Plume EP93A mean concentration ($n = 22$)
TSM (μg/l)	22.3 ± 5.0	58.6 ± 13.8	31.7 ± 15.7	27.5 ± 3.8	14.6 ± 2.8	30.6 ± 10.5	68.3 ± 20.4
Al (nmol/l)	42.7 ± 4.9	63.1 ± 14.8	46.9 ± 22.8	28.7 ± 8.3	18.7 ± 7.9	24.6 ± 7.2	7.4 ± 2.8
Si (nmol/l)	141.0 ± 16.4	233.2 ± 62.9	156.5 ± 72.9	109.4 ± 27.9	75.3 ± 26.7	119.3 ± 29.7	136 ± 46.7
P (nmol/l)	0.78 ± 0.18	35.8 ± 17.7	5.6 ± 0.04	13.4 ± 3.6	0.71 ± 0.23	18.59 ± 10.10	71.8 ± 31.2
S (nmol/l)	6.96 ± 4.95	12.0 ± 6.9	8.1 ± 2.7	3.7 ± 0.8	3.7 ± 0.1	3.6 ± 1.3	8.9 ± 5.2
K (nmol/l)	7.98 ± 2.45	11.32 ± 2.46	8.17 ± 4.05	4.64 ± 1.48	3.08 ± 1.16	4.13 ± 1.14	1.90 ± 0.58
Ca (nmol/l)	19.9 ± 1.95	45.9 ± 13.5	21.6 ± 11.1	29.3 ± 1.9	14.8 ± 3.4	33.3 ± 7.7	68.2 ± 22
Ti (nmol/l)	1.22 ± 0.18	2.03 ± 0.51	1.38 ± 0.70	0.85 ± 0.21	0.53 ± 0.22	0.76 ± 0.21	0.22 ± 0.12
Ba (nmol/l)	0.48 ± 0.05	0.70 ± 0.13	0.51 ± 0.18	0.46 ± 0.05	0.25 ± 0.07	0.36 ± 0.06	0.40 ± 0.11
V (nmol/l)	0.063 ± 0.016	0.64 ± 0.28	0.14 ± 0.14	0.25 ± 0.05	0.03 ± 0.005	0.34 ± 0.18	0.87 ± 0.36
Cr (nmol/l)	0.062 ± 0.009	0.40 ± 0.18	0.11 ± 0.09	0.16 ± 0.03	0.03 ± 0.02	0.20 ± 0.10	0..79 ± 0.36
Mn (nmol/l)	1.66 ± 0.31	1.40 ± 0.27	1.30 ± 0.62	0.80 ± 0.24	0.84 ± 0.26	0.76 ± 0.17	0.53 ± 0.26
Fe (nmol/l)	14.5 ± 1.9	206.6 ± 93.0	44.0 ± 48.1	74.2 ± 15.6	7.9 ± 3.2	106.3 ± 58.2	327.9 ± 140.0
Cu (nmol/l)	0.07 ± 0.06	0.42 ± 0.19	0.19 ± 0.11	0.09 ± 0.03	0.07 ± 0.01	0.11 ± 0.05	0.58 ± 0.50
Zn (nmol/l)	0.19 ± 0.13	0.50 ± 0.26	1.06 ± 0.68	0.19 ± 0.16	0.07 ± 0.01	0.14 ± 0.05	0.18 ± 0.10
As (nmol/l)	0.018 ± 0.018	0.34 ± 0.17	0.06 ± 0.09	0.13 ± 0.04	ND	0.19 ± 0.11	0.64 ± 0.28

Mean ratio							
Al/Fe	2.95 ± 0.16	0.35 ± 0.13	1.35 ± 0.78	0.39 ± 0.08	2.37 ± 0.06	0.29 ± 0.14	0.026 ± 0.01
Si/Fe	9.73 ± 0.41	1.27 ± 0.41	7.31 ± 4.50	1.48 ± 0.26	9.67 ± 0.50	1.36 ± 0.56	0.43 ± 0.10
P/Fe	0.054 ± 0.012	0.17 ± 0.015	0.96 ± 0.04	0.18 ± 0.02	0.092 ± 0.008	0.17 ± 0.01	0.22 ± 0.03
S/Fe	0.49 ± 0.34	0.060 ± 0.029	0.57 ± 0.48	0.05 ± 0.01	0.51 ± 0.19	0.041 ± 0.018	0.031 ± 0.023
K/Fe	0.52 ± 0.11	0.07 ± 0.03	0.36 ± 0.21	0.09 ± 0.05	0.39 ± 0.01	0.05 ± 0.02	0.006 ± 0.002
Ca/Fe	1.38 ± 0.10	0.24 ± 0.05	0.92 ± 0.53	0.41 ± 0.07	1.96 ± 0.36	0.37 ± 0.12	0.22 ± 0.04
Ti/Fe	0.084 ± 0.005	0.011 ± 0.004	0.06 ± 0.03	0.012 ± 0.002	0.067 ± 0.001	0.009 ± 0.004	0.0012 ± 0.0006
Ba/Fe	0.033 ± 0.004	0.0040 ± 0.0014	0.027 ± 0.020	0.006 ± 0.001	0.032 ± 0.004	0.0043 ± 0.002	0.0013 ± 0.0006
V/Fe	0.0043 ± 0.0008	0.0031 ± 0.0001	0.0038 ± 0.001	0.0033 ± 0.0002	0.0043 ± 0.0013	0.0032 ± 0.0001	0.0027 ± 0.0001
Cr/Fe	0.0043 ± 0.0005	0.0019 ± 0.0001	0.004 ± 0.002	0.0022 ± 0.0001	0.0038 ± 0.0006	0.0019 ± 0.0001	0.0024 ± 0.0004
Mn/Fe	0.115 ± 0.02	0.0082 ± 0.0035	0.058 ± 0.037	0.0109 ± 0.003	0.109 ± 0.011	0.0090 ± 0.0043	0.0021 ± 0.0020
Cu/Fe	0.0048 ± 0.0038	0.0023 ± 0.0007	0.004 ± 0.001	0.0012 ± 0.0003	0.0092 ± 0.0027	0.00113 ± 0.0004	0.0017 ± 0.0011
Zn/Fe	0.045 ± 0.098	0.0027 ± 0.0015	0.024 ± 0.011	0.0024 ± 0.002	0.0098 ± 0.0025	0.0016 ± 0.0009	0.0007 ± 0.0008
As/Fe	0.0012 ± 0.0012	0.0016 ± 0.0003	0.001 ± 0.001	0.0017 ± 0.0003	ND	0.0018 ± 0.0002	0.0019 ± 0.0001

Note: ND = not detected. According to Karlin and Lyle (1986) the underlying Gorda Ridge sediments have approximately the following molar ratios: Al/Fe = 2.57; Si/Fe = 8.33; K/Fe = 0.44; and Ti/Fe = 0.087.

from the event plumes indicates that a principal Fe phase is aggregates comprised of individual Fe ferrihydrite particles ~ 0.1 μm in diameter. These Fe ferrihydrite aggregates were generally larger in EP96B than in EP96A (Fig. 7).

The PFe versus nephelometer intensity trend (Fig. 6a) contrasts with the clear offset in intercepts of TSM versus nephelometer intensity apparent between the GR1 and GR3 data (Fig. 2c). Fig. 6a implies that the scattering efficiency of PFe remained unchanged from GR1 to GR3, while Fig. 2c implies that, for a given TSM value, the scattering efficiency increased from GR1 to GR3. Fig. 6b reveals that for a given PFe concentration, total TSM during GR1 was ~ 10 μg/l greater than during GR3, about the same amount that background TSM during GR1 exceed that during GR3 (Table 1). We speculate, therefore, that the GR1 particulate load included a fraction of Fe-poor, weakly scattering particles not present (or much reduced) during GR3. A possible candidate for this particle fraction was terrestrial organic matter delivered to coastal waters by the remarkably high river runoff of the 1996–97 winter. Pak et al. (1970) have demonstrated that near-surface, organic-rich particles in Oregon coastal waters are much less efficient scatterers than mineral particles.

Based on the strong and consistent correlation between PFe and nephelometer intensity for each cruise, plan view distributions of PFe for the three cruises have been constructed from the nephelometer data and are shown in Fig. 8. They indicate maxima in the region of 42.64–42.70°N during the GR1 cruise. Within EP96, peak concentrations of PFe reached 341 nmol/l at about 2100 m in the plume core against a background of ~ 15 nmol/l. The GR2 EP96B event plume was observed farther to the southwest, and PFe concentrations reached a maximum of only 97 nmol/l at about 2100 m because the plume core was never sampled. During GR3, the core of EP96B was observed beyond the west wall of the ridge at 2100 m and had peak concentrations of PFe that exceeded 212 nmol/l, compared with a background of 8 nmol/l. A 3-dimensional view of the PFe plume (not shown) indicates a largely symmetrical PFe concentration gradient from the central core to the edge of the plume. This gradient is probably the result of mixing processes during the early stages of the event plume formation (Lavelle, 1995). Some smaller plumes at the same depth are located north (42.77°N) and south (42.61°N) of the large event plume. These plumes are also enriched in PFe (60–80 nmol/l) and might be spinoffs from the larger event plume.

Particulate S concentrations, on the other hand, only reached a maximum of about 25 nmol/l during the GR1 cruise and showed a positive correlation with PFe in the plumes. The GR1 samples are about a factor of 3 higher in PS concentrations than the GR2 and GR3 samples. While the positive correlation of PS and PFe indicates that most of the particulate S is in the form of sulfide minerals that were most abundant during the GR1 cruise, the strong excess of PFe over PS suggests that Fe ferrihydrite particles are the most abundant phase within the event plume. A few samples from GR1 show high PS and low PFe in the particles. This occurs when high-temperature hydrothermal fluids release sulfide minerals (Zn- and Cu-sulfides) at the seafloor. Similar enrichments of PS in neutrally buoyant plumes were observed at the 9.77°N site on the northern East Pacific Rise a few months after a seafloor eruption was observed (Lupton et al., 1993; Haymon et al., 1993; Feely et al., 1994b).

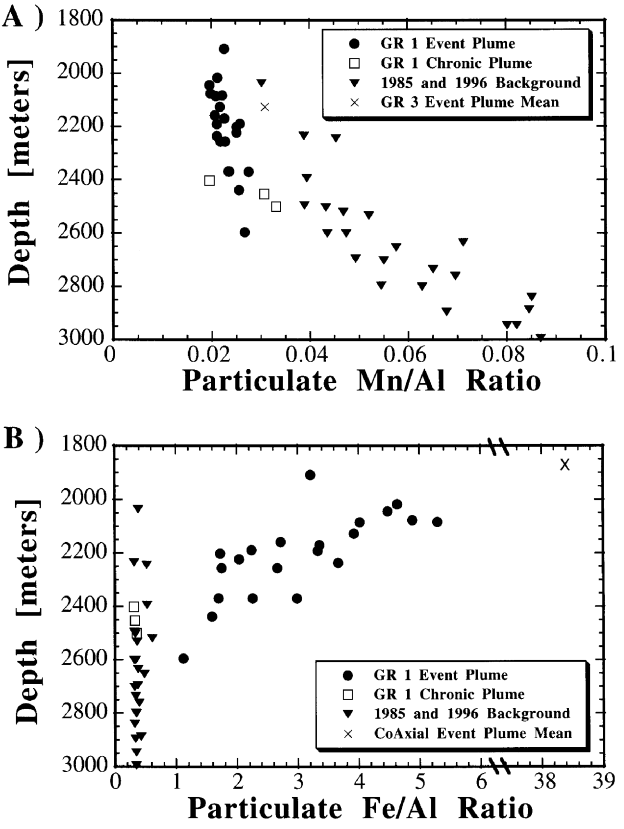

Fig. 5. Vertical profiles of (A) particulate Mn/Al ratio; and (B) particulate Fe/Al ratio for suspended matter within the event and chronic plumes during the GR1 cruise over the Gorda Ridge.

5.3. *Particulate P and V*

The mean concentrations of particulate phosphorus (PP) and particulate vanadium (PV) are given in Table 1. Particulate P concentrations range from < 1 nmol/l in background samples to > 62 nmol/l within the intense hydrothermal plume at 42.67°N during the GR1 cruise. Particulate P concentration peaks, exceeding 35 nmol/l, also occur during the GR3 cruise. These concentrations are more than 80 times background concentrations in the overlying water column. A high degree of correlation exists between PP and PFe during all three GREAT cruises (Fig. 9a). In previous studies, enrichments of PP in hydrothermal particles have been shown to be the result of chemical scavenging of dissolved phosphate from the water column onto Fe ferrihydrite particles (Feely et al., 1990, 1991a, b, 1992, 1994b). The constant slope of the best fit of the three Gorda Ridge data sets (~ 0.18) suggests that once the Fe ferrihydrite particles are formed, the phosphorus concentration in the particles is

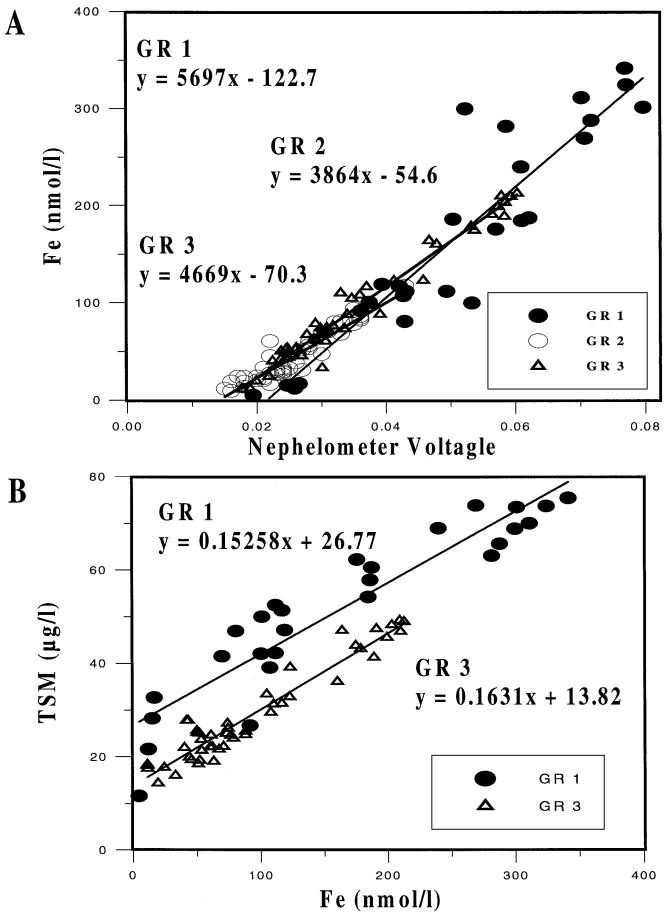

Fig. 6. Plot of particulate iron (PFe) versus nephelometer intensity for the three GREAT cruises (A); and plot of TSM versus PFe for the GR1 and GR3 cruises (B).

determined by the ambient dissolved phosphate concentration (Feely et al., 1991b; Feely et al., 1998). If the total mass of particles settling from the plume is small, this amount of phosphorus enrichment in particles can be measured as a dissolved phosphate anomaly in the water column. Minima in dissolved phosphate are coincident with the PP maxima. The mean dissolved phosphate concentration in the region of the plume maxima at approximately 2100 m over the ridge axis ($\sim$ 2.99 µmol/l) is about 0.064 µmol/l lower than the mean dissolved phosphate concentration at the same depth east of the ridge axis. The large minimum in dissolved phosphate ($>$ 50 nmol/l below background) corresponds with the PP maximum. These anomalies are within a factor of two of the anomalies observed at the hydrothermal

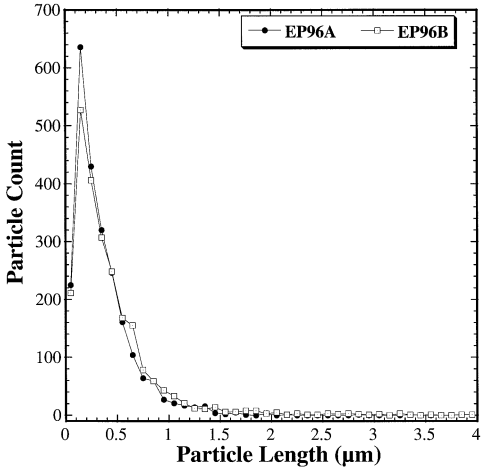

Fig. 7. Particle size distributions of particles and aggregates from EP96A and EP96B. Approximately 2000 particles and aggregates were sized using the Kevex Features Analysis™ software. Note the larger aggregate sizes in the EP96B samples which were collected several weeks after the eruption.

vents on the Juan de Fuca Ridge (Feely et al., 1994a). These data are the first direct evidence for extensive scavenging of dissolved phosphate over this section of the Gorda Ridge.

The PV maxima at 42.64°N reaches values > 1.0 nmol/l, which is about 3.5% of the dissolved V concentrations generally found in the Pacific. The plume maxima for PV are similar to the values in neutrally buoyant plumes over the Juan de Fuca Ridge and mid-Atlantic Ridge (Feely et al., 1994a; Trocine and Trefry, 1989). Since V is readily scavenged from seawater by hydrothermal Fe ferrihydrite particles, these peak values are consistent with the PFe data which also show about the same enrichment over other hydrothermal systems (Fig. 9b). The extent of enrichment is dependent upon the amount of Fe that is available for oxidation to ferrihydrite particles, the residence time of the particles in the water column, and the ambient concentrations of dissolved V and PO4 in seawater (Trefry and Metz, 1989; Feely et al., 1991b).

5.4. Particulate Cu and Zn

Particulate copper (PCu) shows major concentration peaks (> 0.6 nmol/l) within the EP96A event plume, coincident with the PFe peaks. The PCu concentrations from the EP96A samples are about a factor of two higher than the EP96B samples (Fig. 10). Similar factor of two enrichments (not shown) of particulate Zn (PZn) are also observed in the EP96A samples. These enrichments are suggestive of a distinctly unique source for the EP96A event plume samples.

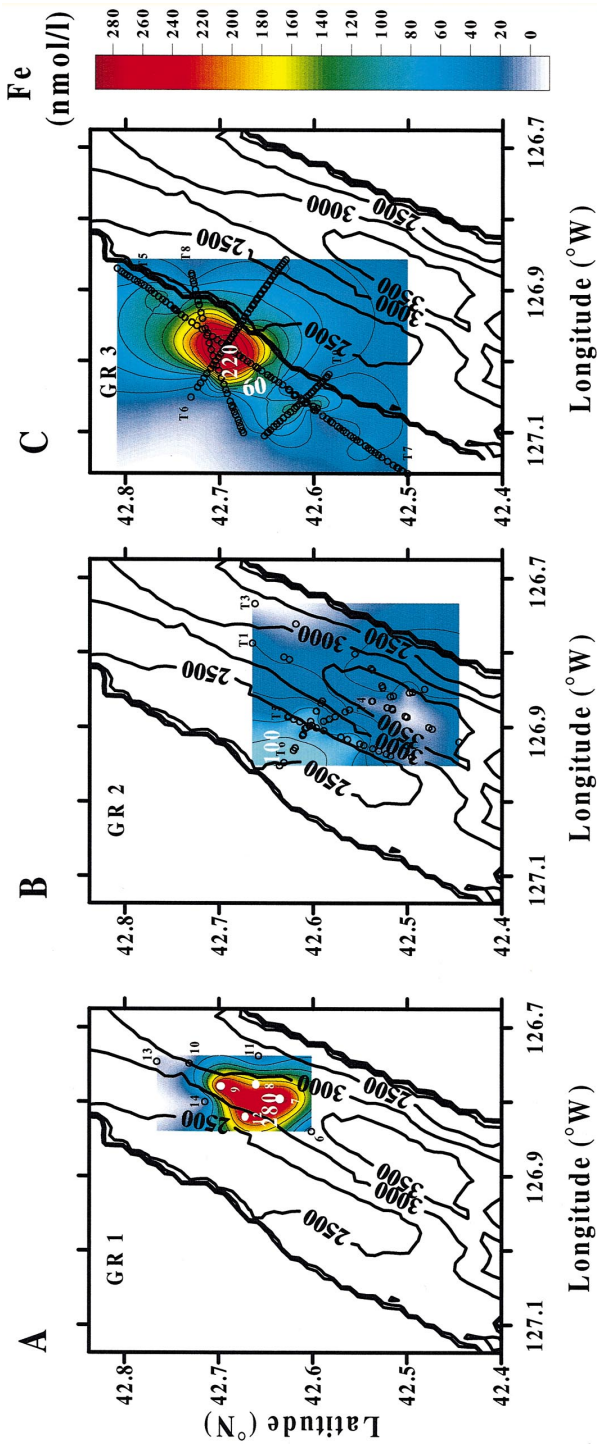

Fig. 8. Plan views of particulate Fe at approximately 2100 m within the event plumes during the three GREAT cruises (*McArthur*, 7–15 March; *Wecoma*, 6–16 April, and *Discoverer*, 10–25 June).

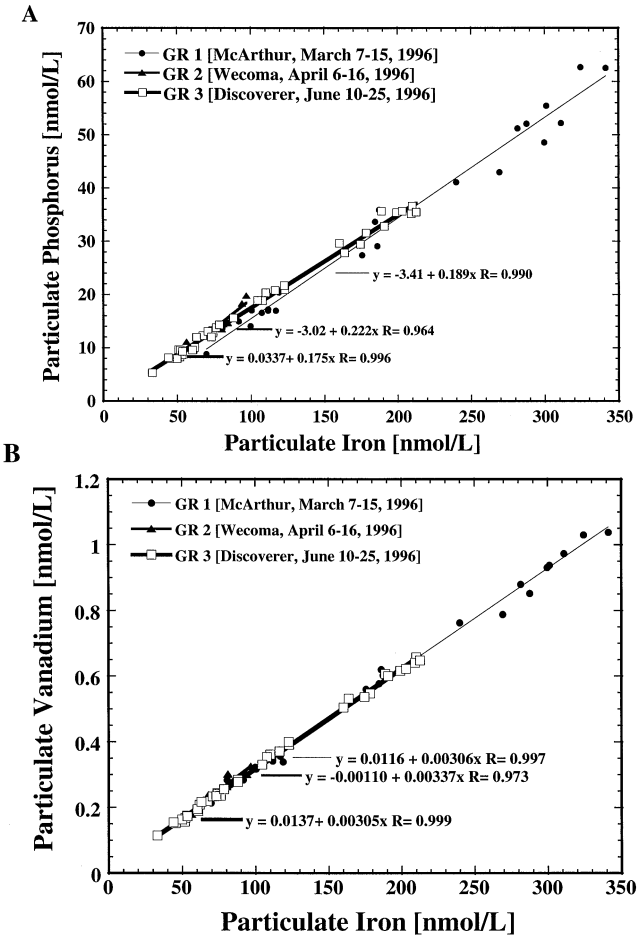

Fig. 9. (A) Scatter diagram of PP versus PFe in the event plumes during the GREAT cruises. (B) Scatter diagram of PV versus PFe in the event plumes during the GREAT cruises. The best-fit lines are not significantly different from each other.

6. Discussion

The compositional differences between the GR1 (EP96A) and the GR2 and GR3 (EP96B) event plume particles (i.e., decreasing Al, S, Mn, Fe, Cu, and Zn concentrations, relatively constant P/Fe and V/Fe ratios, and increased aggregate size) within the Gorda Ridge event plumes may be attributed to: (1) rapid sedimentation of detrital and Cu- and Zn sulfide minerals out of the plume coincident with rapid formation and slow aggregation of Fe ferrihydrite particles within the plume; (2) formation of two

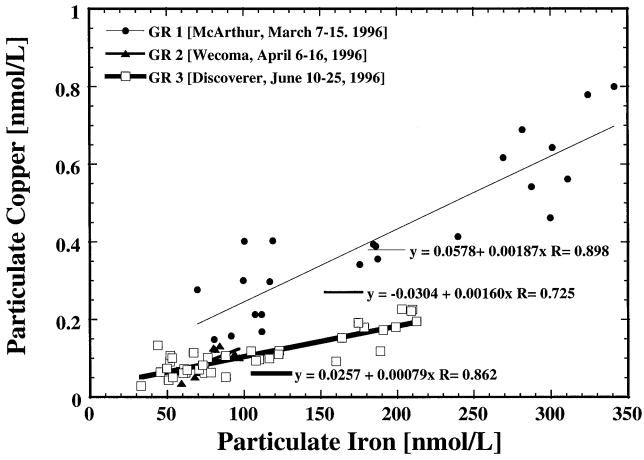

Fig. 10. Scatter diagram of PCu versus PFe in the event plumes during the GREAT cruises. The two-fold enrichment of PCu during the GR1 cruise is significant at the 95% confidence level.

separate event plumes from chemically distinct source fluids followed by slow evolution of the particulate phases; or (3) some combination of both mechanisms. The event plumes were generally dominated by Fe-rich plumes characteristic of seafloor hydrothermal fluids having a strong excess of dissolved Fe over H_2S. A few samples from GR1 show an excess of S over Fe, indicating some evidence for enrichments of Zn- and Cu-sulfide minerals during the massive release of hydrothermal fluids as part of the discharge of fresh lava at the seafloor. H_2S concentrations in vent fluids sometimes exceed Fe concentrations during the early phases of an eruption due to phase separation (Von Damm et al., 1991), with the result that S/Fe ratios in the hydrothermal particles in the water column over the vent fields follow the same trend as the vent fluid ratios (Feely et al., 1994b). The two-fold enrichments of Cu/Fe and Zn/Fe ratios in the event plume particles during GR1 signify an initial release of high temperature vent fluids at the seafloor during the eruption. Since the PCu and PZn concentrations were lower in the EP96B event plume, it is possible that this plume is the product of a possible second lava eruption further to the south. We speculate that this eruption would have released hydrothermal fluids which were significantly lower in Cu and Zn.

These observations are similar to the results from the 9.77°N site on the northern East Pacific Rise, where Cu and Zn-enriched sulfide minerals were observed in the buoyant and neutrally buoyant plumes over the eruption site (Haymon et al., 1993; Feely et al., 1994b; Baron et al., 1998). Our results agree with the conclusions of Baker (1998) that the two eruptions at 42.68°N, 126.78°W and 42.61°N, 126.82°W caused the formation of two separate event plumes; the first (EP96A) being observed during the GR1 cruise, and the second (EP96B) being observed during the GR2 and GR3 cruises.

6.1. Factor analysis of particle chemistry

The analysis of the Gorda Ridge data set consisted of 100 particulate samples collected on the tow-yo and vertical casts from the three GREAT cruises. The samples covered the depth range between 1800 and 3200 m. Fifteen elemental concentrations were used as input for the factor analysis. Three major factors were found, and the oblique factor scores and communality for each element are listed in Table 2. The elements that were found to have high factor 1 scores included those that are normally associated with hydrothermally derived particles, i.e., Fe, P, Ca, V, Cr, Cu, and As. The factor scores for this component have been plotted versus depth in Fig. 11a. The highest scores for this factor are centered on the depth of the event plume maximum, at 2100 m. The scores decrease with depth below the plume, which is consistent with the decrease in the particulate Fe/Al ratio in Fig. 5.

The elements that have high factor 2 scores are all typically found in detrital and resuspended sediment phases (Fig. 11b), including Mn, Al, Si, K, Ti, and Ba. The scores for this factor are low in the region of the event plume maximum and increase almost linearly to the bottom. There is a distinct plume near 2300 m that departs from the linear trend. This region marks a zone of elevated loadings due to the entrainment and uplift of resuspended sediments during the eruption. The factor 1 score for Mn is moderately negative (Table 2). This is because Mn concentrations for the samples that were taken in the event plume are lower than would be predicted based on the values for the other factor 2 elements such as Al or Si. This may be an indication of more than one source for the resuspended sediments or that sedimentary Mn concentrations vary with distance away from the eruption site.

Table 2
Oblique factor loadings for Gorda Ridge event and chronic plumes

Element	Hydrothermal precipitates Factor 1	Resuspended sediments Factor 2	Zinc sulfides Factor 3	Communality
Al	0.002	0.99	0.00	0.982
Si	0.27	0.87	− 0.06	0.960
P	1.05	− 0.11	− 0.03	0.988
S	0.42	0.12	0.48	0.710
K	0.06	0.96	0.01	0.980
Ca	1.01	0.00	− 0.07	0.959
Ti	0.01	0.93	0.02	0.977
Ba	0.10	0.92	0.01	0.938
V	1.02	0.00	− 0.07	0.985
Cr	0.98	0.07	− 0.02	0.982
Mn	− 0.45	1.11	− 0.19	0.876
Fe	1.03	− 0.03	− 0.05	0.986
Cu	0.70	0.20	0.23	0.896
Zn	− 0.25	− 0.20	1.12	0.901
As	1.00	− 0.06	− 0.08	0.955

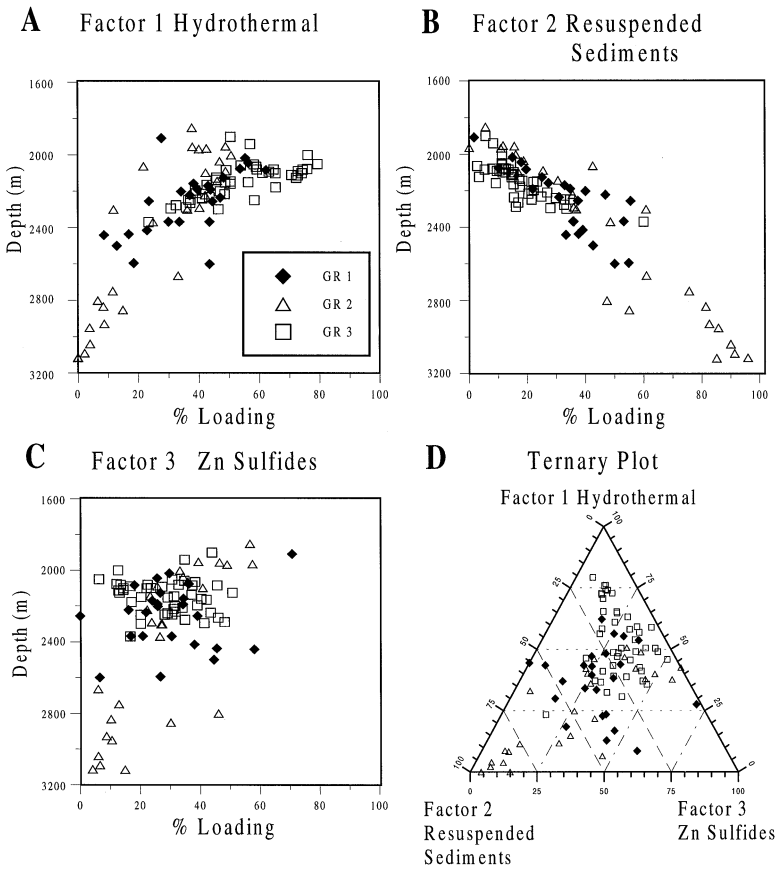

Fig. 11. Plots of oblique factor scores versus depth for the three phases found in the suspended matter over the northern Gorda Ridge: (A) factor 1, (B) factor 2, (C) factor 3, (D) ternary plot of the three factors.

The third factor is composed of high scores for Zn and moderate scores for S and Cu. The loadings for this factor show less structure with depth than the previous factors (Fig. 11c).

The three factor scores were normalized to sum to 100% and then plotted as a ternary plot (Fig. 11d). The plot shows that the maximum percentage of the hydrothermal material increased from GR1 to GR3. This is probably due to the settling dynamics of the particles, since the resuspended aluminosilicates will settle out faster than the Fe ferrihydrite particles.

6.2. Plume inventories for Fe and scavenged P and V

An important finding of this work on the Gorda Ridge event plumes is that Fe-rich ferrihydrite particles comprise the majority of the hydrothermal particles within the

plumes. Since oxyanion species (P, V, Cr, As, etc.) are quickly scavenged from seawater during the formation of the Fe ferrihydrite particles, the event plumes are potentially significant sinks for these chemical species in the oceans. Table 3 summarizes the Fe inventories and the associated scavenged P and V of event plumes on the Juan de Fuca and Gorda Ridges since 1986. The Fe inventories for Juan de Fuca event plumes are taken from the summaries in Massoth et al. (1998). The Fe inventories for the Gorda Ridge event plumes are obtained using two independent methods. In our study, we determined the total amount of PFe in the event plumes by means of an integration of the nephelometer signal within the plumes multiplied by a constant Fe/nephelometer voltage ratio for each cruise. In the case of GR1 only the downcasts were used; for GR3 the tow-yo casts that sampled the plume were used along with one vertical cast. The data from each cruise was then depth averaged in 50 m intervals. Each of these 50 m intervals was then individually gridded using the contouring software package Surfer™ by Golden Software. In both cases, the depth range was the same (1850–2500 m). The coordinates used for the GR1 gridding were from latitude 42.6 to 42.77°N and longitude 126.7 to 126.8°W. Therefore, dimensions of each volume element were about $400 \times 212 \times 50$ m. For GR3, the range of latitude was from 42.5 to 42.8°N, and for longitude from 127.15 to 126.85°W. The software Slicer™ was then used to read the gridded data files and determine the volume elements within the region where event plume PFe concentration exceeded 30 nmol/l (~ 2 times background concentrations). The volumes (a set of concentric shells) for progressively higher Fe concentrations were determined and summed. The total volume for the plume for GR1, which has a PFe concentration > 30 nmol/l, was found to be 105 km^3, with a total Fe inventory of 11×10^6 moles. For GR3, the plume volume was 136 km^3 with an Fe inventory of 9.2×10^6 moles (Table 3).

An alternative estimate of the hydrothermal Fe inventory of event plumes is given by the product of the hydrothermal heat inventory (Baker, 1998) and the total

Table 3
Iron, phosphorus, and vanadium inventories in northeast Pacific event plumes

		Fe[a] mol × 10^6	Fe[b] mol × 10^6	P/Fe	P uptake mol × 10^6	V/Fe	V uptake mol × 10^3
MP I	EP86A	75[c]		0.17	13	0.0023	170
MP II	EP87A	4.1[c]		0.21	0.86	0.0023	9.4
CoAxial A	EP93A	4.0[c]	4.8	0.23	0.9–1.1	0.0026	10–12
CoAxial B	EP93B	7.0[c]		0.23	1.6	0.0026	18
CoAxial C	EP93C	9.0[c]		0.23	2.1	0.0026	23
Gorda Ridge	EP96A	13[c]	11[d]	0.18	2.0	0.0030	33
Gorda Ridge	EP96B	3.5[c]	9.2	0.18	1.7	0.0030	28

[a] Total Fe = (Heat inventory) × (Fe/heat ratio).
[b] Total Particulate Fe = (Nephelometer voltage) × (PFe/nephelometer voltage ratio) × (volume).
[c] Data from Massoth et al. (this issue).
[d] The assumed value for E–W extent of the plume was 10 km.

dissolvable Fe/heat ratio (Massoth et al., 1998). This estimate is 13.0×10^6 mol for EP96A and 3.5×10^6 mol for EP96B (Table 3). While the EP96A values for both methods are reasonably close, the estimate of hydrothermal Fe for EP96B is lower than our estimate for PFe (9.2×10^6 mol) by more than a factor of two. These differences are due principally to different volumetric definitions and integration procedures for the event plumes. The large difference in Fe inventory for EP96B occurs for two reasons. First, the nephelometer signal has greater sensitivity than the temperature anomaly and can thus include the very dilute margins of the event plume where a temperature anomaly cannot be reliably determined. Second, we have included all nephelometer anomalies observed during GR3, whereas Baker (1998) defined EP96B only as anomalies found north of $\sim 46.63°$N (Fig. 4). Our PFe inventory for EP96B may be overestimated owing to the sparseness of data available to the Slicer™ program south of 46.63°N. Calculating mean Fe concentrations for both methods reveals a satisfactory agreement not obvious in the volumetric data. Mean Fe concentrations calculated by the heat inventory method are 102 and 52 nmol/l for EP96A and EP96B, respectively (Massoth et al., 1998). Mean PFe concentrations using the nephelometer integration are 100 and 68 nmol/l for EP96A and EP96B, respectively.

Although the inventory data reported in this paper are for particulate Fe and those by Massoth et al. (1998) for total dissolvable Fe, operationally we expect little difference. Almost all "dissolved Fe" in the neutrally buoyant plume is actually colloidal Fe (Massoth et al., 1994). While these colloids may pass through a clean 0.4 μm Nuclepore™ filter, once larger particles begin to accumulate on the filter surface and overlap the pores the Fe colloids become trapped in the particle matrix.

To obtain the P and V inventories, the corresponding P/Fe and V/Fe ratios for particulate samples from each cruise were multiplied by the respective Fe inventory. For comparison, we also have given the event plume inventories of Juan de Fuca Ridge event plumes (Table 3). The Fe inventories within the known event plumes range from 4.0 to 75×10^6 moles. The two event plumes from the Gorda Ridge total about 20×10^6 moles Fe, which is very similar to the sum of the Fe inventories in the CoAxial event plumes and only about 28% of the Fe in the EP86A event plume at the north Cleft Segment of the Juan de Fuca Ridge. These Fe inventories are similar in size to the chronic plumes observed over the active vent fields on the southern East Pacific Rise between 14° and 19°S (Feely et al., 1996).

The Gorda Ridge event plumes had approximately 80% of the P found in the CoAxial event plumes and about 28% of the P in the EP86A event plume. The range of P inventories within these few event plumes are from about 0.9 to 13×10^6 moles/event. This range of P inventories is a small, but measurable (~ 0.01–0.1%), percentage of the total amount of P removed by hydrothermal processes at ridge crest spreading centers (Wheat et al., 1996). Similar percentages (0.004–0.09%) are obtained when the V inventories are compared with the V removal at ridge crests (Trefry and Metz, 1989). While the number of observations of Fe, P, and V distributions in small and large event plumes is too small to extrapolate these limited results to the global ridge crest system with any degree of confidence, the magnitudes of the Fe, P, and V inventories in these event plumes are large enough to suggest that they could be

potentially significant, provided the frequency of event plume occurrence is high. For example, it would take about 800–8700 event plumes of the sizes measured on the Juan de Fuca and Gorda Ridges to account for all of the ridge crest phosphorus removal in 1 yr. Further research is required to determine size/frequency distributions of magmatically induced event plumes on the global ridge crest system. Until then we cannot evaluate their role in the hydrothermal budgets of these important elements.

7. Conclusions

Magmatic intrusions on the Gorda Ridge produced at least two large oblate spheroid-shaped event plumes (EP96A and EP96B), which were sampled over a 3-month period. We conducted the first detailed major and trace element analysis of event plume particles. Our measurements showed significant decreases in particulate Cu and Zn concentrations ($>100\%$ decreases in Cu/Fe and Zn/Fe ratios) and essentially no change in the P/Fe and V/Fe ratios between the first and second event plumes. These results suggest that chemically distinct source fluids were involved in the formation of the two event plumes. The event plumes were unique in that they contained unusually high concentrations of resuspended detrital mineral phases. This was due to entrainment of a stable nepheloid layer into the event plumes during their formation. This entrainment process contributed to the off-axis transport of resuspended sediments from the Gorda Ridge axial valley to the flank and slope sediments. This process may also be effective in transporting larval forms of vent organisms away from active vent fields. A strong correlation between nephelometer voltage and particulate Fe (PFe) allowed us to estimate the total amount of particulate Fe in the two plumes at approximately 20×10^6 moles of Fe, or $\sim 28\%$ of the Fe in the 1986 Cleft Segment megaplume (EP86A). Based upon the chemical inventories for particulate Fe, P, and V, we suggest that event plumes might play a small role in their geochemical budgets.

Acknowledgements

The authors thank the officers and crew of the NOAA ships *McArthur* and *Discoverer*, and the R.V. *Wecoma* for logistics support. This research was supported by the National Oceanic and Atmospheric Administration through the auspices of the VENTS Program. Contribution numbers 1857 from the Pacific Marine Environmental Laboratory of NOAA and 469 from the University of Washington Joint Institute for the Study of the Atmosphere and Oceans.

References

Baker, E.T., 1998. Patterns of event and chronic hydrothermal venting following a magmatic intrusion: new perspectives from the 1996 Gorda Ridge eruption. Deep-Sea Research II 45, 2599–2618.

Baker, E.T., Piper, D.Z., 1976. Suspended particulate matter: collection by pressure filtration and elemental analysis by thin film X-ray fluorescence. Deep-Sea Research 23, 181–186.

Baker, E.T., Massoth, G.J., Collier, R.W., Trefry, J.H., Kadko, D., Nelsen, T.A., Rona, P.A., Lupton, J.E., 1987. Evidence for high-temperature hydrothermal venting on the Gorda Ridge, northeast Pacific Ocean. Deep-Sea Research 34(8), 1461–1476.

Baker, E.T., Feely, R.A., Mottl, M.J., Sansone, F.J., Wheat, C.G., Resing, J.A., Lupton, J.E., 1994. Hydrothermal plumes along the East Pacific Rise, 8°40′ to 11°50′N: plume distribution and relationship to the apparent magmatic budget. Earth and Planetary Science Letters 128, 1–17.

Baker, E.T., Massoth, G.J., Feely, R.A., Embley, R.W., Thomson, R.E., Burd, B.J., 1995. Hydrothermal event plumes from the CoAxial seafloor eruption site, Juan de Fuca Ridge. Geophysical Research Letters 22(2), 147–150.

Baker, E.T., Massoth, G.J., Feely, R.A., Cannon, G.A., 1998. The rise and fall of the CoAxial hydrothermal site, 1993–1996. Journal of Geophysical Research (in press).

Baron, S., Haymon, R., Feely, R., Von Damm, K., Lebon, G., Lilley, M., 1997. Variations in the elemental composition of buoyant plume particles from high temperature vents on the East Pacific Rise at 9°–10°N: geographic and temporal trends. Earth and Planetary Science Letters (submitted for publication).

Campbell, A.C., 1991. Mineralogy and chemistry of marine particles by synchrotron X-ray spectrometry, mossbauer spectrometry, and plasma-mass spectrometry. Geophysical Monograph Series 63, 375–390.

Chadwick, W.W., Embley, R.W., Shank, T., 1998. The 1996 Gorda Ridge eruption: Geologic mapping, sidescan sonar, and SeaBeam comparison results. Deep-Sea Research II 45, 2547–2569.

Clarke, T.L., 1978. An oblique factor analysis solution for the analysis of mixtures. Mathematical Geology 10, 225–241.

Cowen, J.P. Li, Y.-H., 1991. The influence of a changing bacterial community on trace metal scavenging in a deep-sea particle plume. Journal of Marine Research 49, 517–542.

Cowen, J.P., Massoth, G.J., Feely, R.A., 1990. Scavenging rates of dissolved manganese in a hydrothermal vent plume. Deep-Sea Research 37(10), 1619–1637.

Cowen, J.P., Bentram, M.A., Baker, E.T., Massoth, G.J., Feely, R.A., Summit, M., 1998. Geomicrobial transformation of Mn in Event Plumes: the 1996 Gorda Ridge eruption. Deep-Sea Research II 45, 2713–2737.

Dymond, J., Roth, S.E., 1988. Plume dispersed hydrothermal particles: a time-series record of settling flux from the Endeavor Ridge using moored sensors. Geochimica et Cosmochimica Acta 52, 2525–2536.

Embley, R.W., Chadwick Jr, W.W., Jonasson, I.A., Butterfield, D.A., Baker, E.T., 1995. Initial results of the rapid response to the 1993 CoAxial event: relationships between hydrothermal and volcanic processes. Geophysical Research Letters 22(2), 143–146.

Feely, R.A., Lewison, M.A., Massoth, G.J., Robert Baldo, G., Lavelle, J.W., Byrne, R.H., Von Damm, K.L., Curl Jr, H.C., 1987. Composition and dissolution of black smoker particles from active vents on the Juan de Fuca Ridge. Journal of Geophysical Research 92(11), 11 347–11 363.

Feely, R.A., Massoth, G.J., Baker, E.T., Cowen, J.P., Lamb, M.F., Krogslund, K.A., 1990a. The effect of hydrothermal processes on mid-water phosphorus distributions in the northeast Pacific. Earth and Planetary Science Letters 96, 305–318.

Feely, R.A., Geiselman, T.L., Baker, E.T., Massoth, G.J., Hammond, S.R., 1990b. Distribution and composition of buoyant and non-buoyant hydrothermal plume particles from the ASHES vent at Axial Volcano, Juan de Fuca Ridge. Journal of Geophysical Research 95(B8), 12 855–12 874.

Feely, R.A., Massoth, G.J., Lebon, G.T., 1991a. Sampling of marine particulate matter and analysis by X-ray fluorescence spectrometry. In: Hurd, D.C., Spencer, D.W. (Eds.), Marine Particles: Analysis and Characterization, Geophys. Monogr. Ser., vol. 63, AGU, Washington, DC, pp. 251–257.

Feely, R.A., Trefry, J.H., Massoth, G.J., Metz, S., 1991b. A comparison of the scavenging of phosphorus and arsenic from seawater by hydrothermal iron oxyhydroxides in the Atlantic and Pacific Oceans. Deep-Sea Research 38(6), 617–623.

Feely, R.A., Massoth, G.J., Baker, E.T., Lebon, G.T., Geiselman, T., 1992. Tracking the dispersal of hydrothermal plumes from the Juan de Fuca Ridge using suspended matter compositions. Journal of Geophysical Research 9(B3), 3457–3468.

Feely, R.A., Massoth, G.J., Trefry, J.H., Baker, E.T., Paulson, A.J., Lebon, G.T., 1994a. Composition and sedimentation of hydrothermal plume particles from North Cleft segment, Juan de Fuca Ridge. Journal of Geophysical Research 99(B3), 4985–5006.

Feely, R.A., Gendron, J.F., Baker, E.T., Lebon, G.T., 1994b. Hydrothermal plumes along the East Pacific Rise, 8°40′ to 11°50′N: 3. Particle distribution and composition. Earth and Planetary Science Letters 128, 19–36, 1994b.

Feely, R.A., Baker, E.T., Marumo, K., Urabe, T., Ishibashi, J., Gendron, J., Lebon, G.T., Okamura, K., 1996. Hydrothermal plume particles and dissolved phosphate over the superfast spreading southern East Pacific Rise. Geochimica et Cosmochimica Acta 60(13), 2297–2323.

Feely, R.A., Trefry, J.H., Lebon, G.T., German, C.R., 1998. The relationship between P/Fe and V/Fe ratios in hydrothermal precipitates and dissolved phosphate in seawater. Geophysical Research Letters 25(13), 2253–2256.

Fox, C.G., Dziak, R.P., 1998. Hydroacoustic detection of volcanic activity on the Gorda Ridge, February–March, 1996. Deep-Sea Research II 45, 2513–2530.

Froelich, P.N., Bender, M.L., Heath, G.R., 1977. Phosphorus accumulation rates in metalliferous sediments on the East Pacific Rise. Earth and Planetary Science Letters 34, 351–359.

Froelich, P.N., Bender, M.L., Luedtke, N.A., Heath, G.R., DeVries, T., 1982. The marine phosphorus cycle. American Journal of Science 282, 474–511.

German, C.R., Klinkhammer, G.P., Edmond, J.E., Mitra, A., Elderfield, H., 1990. Hydrothermal scavenging of rare-earth elements in the ocean. Nature 345, 516–518.

German, C.R., Klinkhammer, G.P., Edmond, J.M., Mitra, A., Elderfield, H., 1991a. Hydrothermal scavenging at the Mid-Atlantic Ridge: Radionuclide distributions. Earth and Planetary Science Letters 105, 170–181.

German, C.R., Campbell, A.C., Edmond, J.M., 1991b. Hydrothermal scavenging at the mid-Atlantic Ridge: Modification of trace element dissolved fluxes. Earth and Planetary Science Letters 107, 101–114.

Gardner, W.D., 1977. Incomplete extraction of rapidly settling particles from water samples. Limnology and Oceanography 22, 764–768.

Haymon, R.M. Kastner, M., 1981. Hot spring deposits on the East Pacific Rise at 21°N: Preliminary description of mineralogy and genesis. Earth and Planetary Science Letters 53, 363–381.

Haymon, R.M., Fornari, D.J., Von Damm, K.L., Lilley, M.D., Perfit, M.R., Edmond, J.E., Shanks, III, W.C., Lutz, R.A., Grebmeier, J.M., Carbotte, S., Wright, D., McLaughlin, E., Smith, M., Beedle, N., Olson, E., 1993. Volcanic eruption of the mid-ocean ridge along the East Pacific Rise Crest at 9°45–52′N: direct submersible observations of seafloor phenomena associated with an eruption event in April 1991. Earth and Planetary Science Letters 119, 85–101.

Holmes, G.S., 1981. The limitations of accurate "thin film" X-ray fluorescence analysis of natural particulate matter; problems and solutions. Chemical Geology 33, 333–353.

Kadko, D., Feely, R., Massoth, G., 1994. Scavenging of ^{234}Th and phosphorus removal from the hydrothermal effluent plume over the North Cleft segment of the Juan de Fuca Ridge. Journal of Geophysical Research 99(B3), 5017–5024.

Karlin, R., Lyle, M., 1986. Sediment studies on the Gorda Ridge. State of Oregon Department of Geology and Mineral Industries, Open File Report O-86-19, 76 pp.

Klovan, J.E., Imbrie, J., 1971. An algorithm and Fortran-IV program for large-scale Q-mode factor analysis and calculation of factor scores. Mathematical Geology 3, 61–77.

Leinen, M., Pisias, N., 1984. An objective technique for determining end-member compositions and for partitioning sediments according to their sources. Geochimica et Cosmochimica Acta 48, 47–62.

Lavelle, J.W., 1995. The initial rise of a hydrothermal plume from a line segment source—results from a three-dimensional numerical model. Geophysical Research Letters 22, 159–162.

Leinen, M., 1985. Mineralogy of hydrothermal precipitates within and near active vents on the Juan de Fuca and Explorer Ridges. EOS, Transactions of the American Geophysical Union 66(46), 928.

Lupton, J.E., Baker, E.T., Mottl, M.J., Sansone, E.J., Wheat, C.G., Resing, J.A., Massoth, G.J., Measures, C.J., Feely, R.A., 1993. Chemical and physical diversity of hydrothermal plumes along the east Pacific Rise, 8°45′ to 11°50′N. Geophysical Research Letters 20(24), 2913–2916.

Lupton, J.E., Baker, E.T., Garfield, N., Massoth, G.J., Feely, R.A., Greene, R., Rago, T., 1998. Tracking the evolution of a hydrothermal event plume along a RAFOS neutrally buoyant drifter. Science 280, 1052–1055.

Massoth, G.J., Baker, E.T., Feely, R.A., Butterfield, D.A., Embley, R.W., Lupton, J.E., Thomson, R.E., Cannon, G.A., 1995. Observations of manganese and iron at the CoAxial seafloor eruption site, Juan de Fuca Ridge. Geophysical Research Letters 22(2), 151–154.

Massoth, G.J., Baker, E.T., Feely, R.A., Lupton, J.E., Collier, R.W., Gendron, J.F., Roe, K.K., Maenner, S.M., Resing, J.A., 1998. Manganese and iron in hydrothermal plumes resulting from the 1996 Gorda Ridge event. Deep-Sea Research II 45, 2683–2712.

Metz, S., Trefry, J.H., 1993. Field and laboratory studies of metal uptake and release by hydrothermal precipitates. Journal of Geophysical Research 98(B6), 9961–9666.

Mottl, M.J., 1983. Metabasalts, Axial hot springs, and the structure of hydrothermal systems at mid-ocean ridges. Geological Society of America Bulletin 94, 161–180.

Mottl, M.J., McConachy, T.F., 1990. Chemical processes in buoyant hydrothermal plumes on the East Pacific Rise near 21°N. Geochimica et Cosmochimica Acta 54, 1911–1927.

Pak, H., Beardsley Jr, G.F., Heath, G.R., Curl, H, 1970. Light-scattering vectors of some marine particles. Limnology and Oceanography 15, 683–687.

Trefry, J.H., Metz, S., 1989. Role of hydrothermal precipitates in the geochemical cycling of vanadium. Nature 342, 531–533.

Rona, P.A., Denlinger, R.P., Fisk, M.R., Howard, K.J., Taghon, G.L., Klitgord, K.D., McClain, J.S., McMurtry, G.R., Whitshire, J.C., 1990. Major off-axis hydrothermal activity on the northern Gorda Ridge. Geology 18, 493–496.

Trocine, R.P., Trefry, J.H., 1988. Distribution and chemistry of suspended particles from an active hydrothermal vent site on the Mid-Atlantic Ridge at 26°N. Earth and Planetary Science Letters 88, 1–15.

Von Damm, K.L., Grebmeier, J.M., Edmond, J.M., 1991. Preliminary chemistry of hydrothermal vent fluids from 9–10°N on the East Pacific Rise. EOS, Transactions of the American Geophysical Union 72, 481.

Wheat, C.G., Feely, R.A., Mottl, M.J., 1996. Phosphate removal by hydrothermal processes: an update of the phosphorus budget in the oceans. Geochimica et Cosmochimica Acta 60(19), 3593–3608.